



1 **Groundwater storage dynamics in the world's large aquifer systems**
2 **from GRACE: uncertainty and role of extreme precipitation**

3 **Mohammad Shamsudduha^{1,2,*} and Richard G. Taylor¹**

4 ¹ Department of Geography, University College London, London, UK

5 ² Department of Geography, University of Sussex, Falmer, Brighton, UK

6 * Corresponding author: M. Shamsudduha (M.Shamsudduha@sussex.ac.uk)

7

8 **Abstract**

9 Under variable and changing climates groundwater storage sustains vital ecosystems and
10 enables freshwater withdrawals globally for agriculture, drinking-water, and industry. Here,
11 we assess recent changes in groundwater storage (Δ GWS) from 2002 to 2016 in 37 of the
12 world's large aquifer systems using an ensemble of datasets from the Gravity Recovery and
13 Climate Experiment (GRACE) and Land Surface Models (LSMs). Ensemble GRACE-
14 derived Δ GWS is well reconciled to in-situ observations ($r = 0.62$ – 0.86 , p value <0.001) for
15 two tropical basins with regional piezometric networks and contrasting climate regimes.
16 Trends in GRACE-derived Δ GWS are overwhelmingly non-linear; indeed linear declining
17 trends adequately ($R^2 >0.5$, p value <0.001) explain variability in only two aquifer systems.
18 Non-linearity in Δ GWS at the scale of GRACE ($\sim 200,000$ km²) derives, in part, from the
19 episodic nature of groundwater replenishment associated with extreme annual ($>90^{\text{th}}$
20 percentile, 1901–2016) precipitation and is inconsistent with prevailing narratives of global-
21 scale groundwater depletion. Substantial uncertainty remains in estimates of GRACE-derived
22 Δ GWS, evident from 20 realisations presented here, but these data provide a regional context
23 to changes in groundwater storage observed more locally through piezometry.

24



25 **1 Introduction**

26 Groundwater is estimated to supply substantial proportions of the world's agricultural (42%),
27 domestic (36%), and industrial (27%) freshwater demand (Döll et al., 2012). As the world's
28 largest distributed store of freshwater, groundwater also plays a vital role in sustaining
29 ecosystems and enabling adaptation to increased variability in rainfall and river discharge
30 brought about by climate change (Taylor et al., 2013a). Sustained reductions in the volume of
31 groundwater (i.e. groundwater depletion) resulting from human withdrawals or changes in
32 climate have historically been observed as declining groundwater levels recorded in wells
33 (Scanlon et al., 2012a; Castellazzi et al., 2016; MacDonald et al., 2016). The limited
34 distribution and duration of piezometric records hinder, however, direct observation of
35 changes in groundwater storage globally including many of the world's large aquifer systems
36 (WHYMAP and Margat, 2008).

37 Since 2002 the Gravity Recovery and Climate Experiment (GRACE) has enabled large-scale
38 ($\geq 200,000 \text{ km}^2$) satellite monitoring of changes in total terrestrial water storage (ΔTWS)
39 globally (Tapley et al., 2004). As the twin GRACE satellites circle the globe ~15 times a day
40 they measure the inter-satellite distance at a minute precision (within one micron) and
41 provide ΔTWS for the entire earth approximately every 30 days. GRACE satellites sense
42 movement of total terrestrial water mass derived from both natural (e.g. droughts) and
43 anthropogenic (e.g. irrigation) influences globally (Rodell et al., 2018). Changes in
44 groundwater storage (GRACE-derived ΔGWS) are computed from ΔTWS after deducting
45 contributions (equation 1) that arise from other terrestrial water stores including soil moisture
46 (ΔSMS), surface water (ΔSWS), and the snow water storage (ΔSNS) using data from Land
47 Surface Models (LSMs) either exclusively (Rodell et al., 2009; Famiglietti et al., 2011;
48 Scanlon et al., 2012a; Famiglietti and Rodell, 2013; Richey et al., 2015; Thomas et al., 2017)



49 or in combination with in situ observations (Rodell et al., 2007; Swenson et al., 2008;
50 Shamsudduha et al., 2012).

$$51 \quad \Delta GWS = \Delta TWS - (\Delta SMS + \Delta SWS + \Delta SNS) \quad (1)$$

52 Substantial uncertainty persists in the quantification of changes in terrestrial water stores
53 from GRACE measurements that are limited in duration (2002 to 2016), and the application
54 of uncalibrated, global-scale LSMs (Shamsudduha et al., 2012; Döll et al., 2014; Scanlon et
55 al., 2018). Computation of ΔGWS from GRACE ΔTWS is argued, nevertheless, to provide
56 evaluations of large-scale changes in groundwater storage where regional-scale piezometric
57 networks do not currently exist (Famiglietti, 2014).

58 Previous assessments of changes in groundwater storage using GRACE in the world's 37
59 large aquifer systems (Richey et al., 2015; Thomas et al., 2017) (Fig. 1, Table 1) have raised
60 concerns about the sustainability of human use of groundwater resources. One analysis
61 (Richey et al., 2015) employed a single GRACE ΔTWS product (CSR) in which changes in
62 subsurface storage ($\Delta SMS + \Delta GWS$) were attributed to ΔGWS . This study applied linear
63 trends without regard to their significance to compute values of GRACE-derived ΔGWS over
64 11 years from 2003 to 2013, and concluded that the majority of the world's aquifer systems
65 ($n=21$) are either "overstressed" or "variably stressed". A subsequent analysis (Thomas et al.,
66 2017) employed a different GRACE ΔTWS product (Mascons) and estimated ΔSWS from
67 LSM data for both surface and subsurface runoff, though the latter is normally considered to
68 be groundwater recharge (Rodell et al., 2004). Using performance metrics normally applied
69 to surface water systems including dams, this latter analysis classified nearly a third ($n=11$) of
70 the world's aquifer systems as having their lowest sustainability criterion.

71 Here, we update and extend the analysis of ΔGWS in the world's 37 large aquifer systems
72 using an ensemble of three GRACE ΔTWS products (CSR, Mascons, GRGS) over a 14-year



73 period from August 2002 to July 2016. To isolate GRACE-derived Δ GWS from GRACE
74 Δ TWS, we employ estimates of Δ SMS, Δ SWS and Δ SNS from five LSMs (CLM, Noah,
75 VIC, Mosaic, Noah v.2.1) run by NASA's Global Land Data Assimilation System (GLDAS).
76 As such, we explicitly account for the contribution of Δ SWS to Δ TWS, which has been
77 commonly overlooked (Rodell et al., 2009; Richey et al., 2015; Bhanja et al., 2016) despite
78 evidence of its significant contribution to Δ TWS (Kim et al., 2009; Shamsudduha et al.,
79 2012; Getirana et al., 2017). Further, we characterise trends in time-series records of
80 GRACE-derived Δ GWS by employing a non-parametric, Seasonal-Trend decomposition
81 procedure based on Loess (STL) (Cleveland et al., 1990) that allows for resolution of
82 seasonal, trend and irregular components of GRACE-derived Δ GWS for each large aquifer
83 system. In contrast to linear or multiple-linear regression-based techniques, STL assumes
84 neither that data are normally distributed nor that the underlying trend is linear
85 (Shamsudduha et al., 2009; Humphrey et al., 2016; Sun et al., 2017).

86

87 **2 Data and Methods**

88 **2.1 Global large aquifer systems**

89 We use the World-wide Hydrogeological Mapping and Assessment Programme (WHYMAP)
90 Geographic Information System (GIS) dataset for the delineation of world's 37 Large Aquifer
91 Systems (Fig. 1, Table1) (WHYMAP and Margat, 2008). The WHYMAP network, led by
92 the German Federal Institute for Geosciences and Natural Resources (BGR), serves as a
93 central repository and hub for global groundwater data, information, and mapping with a goal
94 of assisting regional, national, and international efforts toward sustainable groundwater
95 management (Richts et al., 2011). The largest aquifer system in this dataset (Supplementary
96 Table S1) is the East European Aquifer System (WHYMAP no. 33; area: 2.9 million km²)



97 and the smallest one the California Central Valley Aquifer System (WHYMAP no. 16; area:
98 71,430 km²), which is smaller than the typical sensing area of GRACE (~200,000 km²).
99 However, Longuevergne et al. (2013) argue that GRACE satellites are sensitive to total mass
100 changes at a basin scale so Δ TWS measurements can be applied to smaller basins if the
101 magnitude of temporal mass changes is substantial due to mass water withdrawals (e.g.,
102 intensive groundwater-fed irrigation). Mean and median sizes of these large aquifers are
103 ~945,000 km² and ~600,000 km², respectively.

104 **2.2 GRACE products**

105 We use post-processed, gridded ($1^\circ \times 1^\circ$) monthly GRACE TWS data from CSR land
106 (Landerer and Swenson, 2012) and JPL Global Mascon (Watkins et al., 2015; Wiese et al.,
107 2016) solutions from NASA's dissemination site (<http://grace.jpl.nasa.gov/data>), and a third
108 GRGS GRACE solution (CNES/GRGS release RL03-v1) (Biancale et al., 2006) from the
109 French Government space agency, Centre National D'études Spatiales (CNES). To address
110 the uncertainty associated with different GRACE processing strategies (CSR, JPL-Mascons,
111 GRGS), we apply an ensemble mean of the three GRACE solutions (Bonsor et al., 2018).

112 CSR land solution (version RL05.DSTvSCS1409) is post-processed from spherical
113 harmonics released by the Centre for Space Research (CSR) at the University of Texas at
114 Austin. CSR gridded datasets are available at a monthly timestep and a spatial resolution of
115 $1^\circ \times 1^\circ$ (~111 km at equator) though the actual spatial resolution of GRACE footprint
116 (Scanlon et al., 2012a) is 450 km \times 450 km or ~200,000 km². To amplify TWS signals we
117 apply the dimensionless scaling factors provided as $1^\circ \times 1^\circ$ bins that are derived from
118 minimising differences between TWS estimated from GRACE and the hydrological fields
119 from the Community Land Model (CLM4.0) (Landerer and Swenson, 2012). JPL-Mascons
120 (version RL05M_1.MSCNv01) data processing involves the same glacial isostatic adjustment



121 correction but applies no spatial filtering as JPL-RL05M directly relates inter-satellite range-
122 rate data to mass concentration blocks (mascons) to estimate monthly gravity fields in terms
123 of equal area $3^\circ \times 3^\circ$ mass concentration functions in order to minimise measurement errors.
124 Gridded mascon fields are provided at a spatial sampling of 0.5° in both latitude and
125 longitude (~ 56 km at the equator). Similar to CSR product, dimensionless scaling factors are
126 provided as $0.5^\circ \times 0.5^\circ$ bins (Shamsudduha et al., 2017) to apply to the JPL-Mascons product
127 that also derive from the Community Land Model (CLM4.0) (Wiese et al., 2016). The scaling
128 factors are multiplicative coefficients that minimize the difference between the smoothed and
129 unfiltered monthly Δ TWS variations from the CLM4.0 hydrology model (Wiese et al., 2016).
130 Finally, GRGS GRACE (version RL03-v1) monthly gridded solutions of a spatial resolution
131 of $1^\circ \times 1^\circ$ are extracted and aggregated time-series data are generated for each aquifer
132 system. A description of the estimation method of Δ GWS from GRACE and in-situ
133 observations is provided below.

134 **2.3 Estimation of Δ GWS from GRACE**

135 We apply monthly measurements of terrestrial water storage anomalies (Δ TWS) from
136 Gravity Recovery and Climate Experiment (GRACE) satellites, and simulated records of soil
137 moisture storage (Δ SMS), surface runoff or surface water storage (Δ SNS) and snow water
138 equivalent (Δ SNS) from NASA's Global Land Data Assimilation System (GLDAS version
139 1.0) at $1^\circ \times 1^\circ$ grids for the period of August 2002 to July 2016 to estimate (equation 1)
140 groundwater storage changes (Δ GWS) in the 37 WHYMAP large aquifer systems. This
141 approach is consistent with previous global (Thomas et al., 2017) and basin-scale (Rodell et
142 al., 2009; Asoka et al., 2017; Feng et al., 2018) analyses of Δ GWS from GRACE. We apply 3
143 gridded GRACE products (CSR, JPL-Mascons, GRGS) and an ensemble mean of Δ TWS and
144 individual storage component of Δ SMS and Δ SWS from 4 Land Surface Models (LSMs):
145 CLM, Noah, VIC, Mosaic), and a single Δ SNS from Noah model (GLDAS version 2.1) to



146 derive a total of 20 realisations of ΔGWS for each of the 37 aquifer systems. We then
147 averaged all the GRACE-derived ΔGWS estimates to generate an ensemble mean ΔGWS
148 time-series record for each aquifer system. GRACE and GLDAS LSMs derived datasets are
149 processed and analysed in R programming language (R Core Team, 2017).

150 **2.4 GLDAS Land Surface Models**

151 To estimate GRACE-derived ΔGWS using equation (1), we use simulated soil moisture
152 storage (ΔSMS), surface runoff, as a proxy for surface water storage ΔSWS (Getirana et al.,
153 2017; Thomas et al., 2017), and snow water equivalent (ΔSNS) from NASA's Global Land
154 Data Assimilation System (GLDAS). GLDAS system (<https://ldas.gsfc.nasa.gov/gldas/>)
155 drives multiple, offline (not coupled to the atmosphere) Land Surface Models globally
156 (Rodell et al., 2004), at variable grid resolutions (from 2.5° to 1 km), enabled by the Land
157 Information System (LIS) (Kumar et al., 2006). Currently, GLDAS (version 1) drives four
158 land surface models (LSMs): Mosaic, Noah, the Community Land Model (CLM), and the
159 Variable Infiltration Capacity (VIC). We apply monthly ΔSMS (sum of all soil profiles) and
160 ΔSWS data at a spatial resolution of $1^\circ \times 1^\circ$ from 4 GLDAS LSMs: the Community Land
161 Model (CLM, version 2.0) (Dai et al., 2003), Noah (version 2.7.1) (Ek et al., 2003), the
162 Variable Infiltration Capacity (VIC) model (version 1.0) (Liang et al., 2003), and Mosaic
163 (version 1.0) (Koster and Suarez, 1992). The respective total depths of modelled soil profiles
164 are 3.4 m, 2.0 m, 1.9 m and 3.5 m in CLM (10 vertical layers), Noah (4 vertical layers), VIC
165 (3 vertical layers), and Mosaic (3 vertical layers) (Rodell et al., 2004). For snow water
166 equivalent (ΔSNS), we use simulated data from Noah (v.2.1) model (GLDAS version 2.1)
167 that is forced by the global meteorological data set from Princeton University (Sheffield et
168 al., 2006); LSMs under GLDAS (version 1) are forced by the CPC Merged Analysis of
169 Precipitation (CMAP) data (Rodell et al., 2004).



170 **2.5 Global precipitation datasets**

171 To evaluate the relationships between precipitation and GRACE-derived Δ GWS, we use a
172 high-resolution (0.5 degree) gridded, global precipitation dataset (version 4.01) (Harris et al.,
173 2014) available from the Climatic Research Unit (CRU) at the University of East Anglia
174 (<https://crudata.uea.ac.uk/cru/data/hrg/>). In light of uncertainty in observed precipitation
175 datasets globally, we test the robustness of relationship between precipitation and
176 groundwater storage using the GPCC (Global Precipitation Climatology Centre) precipitation
177 dataset (Schneider et al., 2017) (<https://www.esrl.noaa.gov/psd/data/gridded/data.gpcc.html>)
178 from 1901 to 2016. Time-series (January 1901 to July 2016) of monthly precipitation from
179 CRU and GPCC datasets for the WHYMAP aquifer systems were analysed and processed in
180 R programming language (R Core Team, 2017).

181 **2.6 Seasonal-Trend Decomposition (STL) of GRACE Δ GWS**

182 Monthly time-series records (Aug 2002 to Jul 2016) of the ensemble mean GRACE Δ TWS
183 and GRACE-derived Δ GWS were decomposed to seasonal, trend and remainder or residual
184 components using a non-parametric time series decomposition technique known as
185 ‘Seasonal-Trend decomposition procedure based on a locally weighted regression method
186 called LOESS (STL)’ (Cleveland et al., 1990). Loess is a nonparametric method so that the
187 fitted curve is obtained empirically without assuming the specific nature of any structure that
188 may exist within the data (Jacoby, 2000). A key advantage of STL method is that it reveals
189 relatively complex structures in time-series data that could easily be overlooked using
190 traditional statistical methods such as linear regression.

191 STL decomposition technique has previously been used to analyse GRACE Δ TWS regionally
192 (Hassan and Jin, 2014) and globally (Humphrey et al., 2016). GRACE-derived Δ GWS time-



193 series records for each aquifer system were decomposed using the STL method (see equation
194 2) in the R programming language (R Core Team, 2017) as:

$$195 \quad Y_t = T_t + S_t + R_t \quad (2)$$

196 where Y_t is the monthly Δ GWS at time t , T_t is the trend component; S_t is the seasonal
197 component; and R_t is an remainder (residual or irregular) component.

198 The STL method consists of a series of smoothing operations with different moving window
199 widths chosen to extract different frequencies within a time series, and can be regarded as an
200 extension of classical methods for decomposing a series into its individual components
201 (Chatfield, 2003). The nonparametric nature of the STL decomposition technique enables
202 detection of nonlinear patterns in long-term trends that cannot be assessed through linear
203 trend analyses (Shamsudduha et al., 2009). For STL decomposition, it is necessary to choose
204 values of smoothing parameters to extract trend and seasonal components. Selection of
205 parameters in STL decomposition is a subjective process. The choice of the seasonal
206 smoothing parameter determines the extent to which the extracted seasonal component varies
207 from year to year: a large value will lead to similar components in all years whereas a small
208 value will allow the extracted component to track the observations more closely. Similar
209 comments apply to the choice of smoothing parameter for the trend component. We
210 experimented with several different choices of smoothing parameters at a number of
211 contrasting sites and checked the residuals (i.e. remainder component) for the overall
212 performance of the STL decomposition model. Visualization of the results with several
213 smoothing parameters suggested that the overall structure of time series at all sites could be
214 captured reasonably using window widths of 13 for the seasonal component and 37 for the
215 trend. We apply the STL decomposition with a robust fitting of the loess smoother
216 (Cleveland et al., 1990) to ensure that the fitting of the curvilinear trend does not have an



217 adverse effect due to extreme outliers in the time-series data (Jacoby, 2000). Finally, to make
218 the interpretation and comparison of nonlinear trends across all 37 aquifer systems,
219 smoothing parameters were then fixed for all subsequent STL analyses.

220

221 **3 Results**

222 **3.1 Variability in Δ TWS of the large aquifer systems**

223 Ensemble mean time series of GRACE Δ TWS for the world's 37 large aquifer systems are
224 shown in Fig. 2 (High Plains Aquifer System, no. 17) and supplementary Figs. S1-S36 for the
225 other 36 aquifer systems. The STL decomposition of an ensemble GRACE Δ TWS in the
226 High Plains Aquifer System (no. 17) decomposes the time series into seasonal, trend and
227 residual components (see supplementary Fig. S37). Variance (square of the standard
228 deviation) in monthly GRACE Δ TWS (Supplementary Table S1, Figs. 3a and 4) is highest
229 ($>100 \text{ cm}^2$) primarily under monsoonal precipitation regimes within the Inter-Tropical
230 Convergence Zone (e.g. Upper Kalahari-Cuvelai-Zambezi-11, Amazon-19, Maranhão-20,
231 Ganges-Brahmaputra-24). The sum of individual components derived from the STL
232 decomposition (i.e., seasonal, trend and irregular or residual) approximates the overall
233 variance in time-series data. The majority of the variance ($>50\%$) in Δ TWS is explained by
234 seasonality (Fig. 3a); non-linear (curvilinear) trends represent $<25\%$ of the variance in Δ TWS
235 with the exception of the Upper Kalahari-Cuvelai-Zambezi-11 (42%). In contrast, variance in
236 GRACE Δ TWS in most hyper-arid and arid basins is low (Fig. 3a), $<10 \text{ cm}^2$ (e.g., Nubian-1,
237 NW Sahara-2, Murzuk-Djado-3, Taodeni-Tanezrouft-4, Ogaden-Juba-9, Lower Kalahari-
238 Stampriet-12, Karoo-13, Tarim-31) and largely ($> 65\%$) attributed to Δ GWS (Supplementary
239 Table S2). Overall, changes in Δ TWS (i.e., difference between two consecutive hydrological
240 years) are correlated (Pearson correlation, $r > 0.5$, p value < 0.01) to annual precipitation for



241 25 of the 37 large aquifer systems (Table S1). GRACE Δ TWS in aquifer systems under
242 monsoonal precipitation regimes is strongly correlated to rainfall with a lag of 2 months (r
243 >0.65 , p value <0.01).

244 **3.2 GRACE- Δ GWS and evidence from in-situ piezometry**

245 Evaluations of computed GRACE-derived Δ GWS using in situ observations are limited
246 spatially and temporally by the availability of piezometric records (Swenson et al., 2006;
247 Strassberg et al., 2009; Scanlon et al., 2012b; Shamsudduha et al., 2012; Panda and Wahr,
248 2015; Feng et al., 2018). Consequently, comparisons of GRACE and in situ Δ GWS remain
249 opportunity-driven and, here, comprise the Limpopo Basin in South Africa and Bengal Basin
250 in Bangladesh where we possess time series records of adequate duration and density. The
251 Bengal Basin is a part of the Ganges-Brahmaputra aquifer system (aquifer no. 24), whereas,
252 the Limpopo Basin is located between the Lower Kalahari-Stampriet Basin (aquifer no. 12)
253 and the Karoo Basin (aquifer no. 13). The two basins feature contrasting climates (i.e.
254 tropical humid versus tropical semi-arid) and geologies (i.e. unconsolidated sands versus
255 weathered crystalline rock) that represent key controls on the magnitude and variability
256 expected in Δ GWS. Both basins are in the tropics and, as such, serve less well to test the
257 computation of GRACE-derived Δ GWS at mid and high latitudes.

258 In the Bengal Basin, computed GRACE and in situ Δ GWS demonstrate an exceptionally
259 strong seasonal signal associated with monsoonal recharge that is amplified by dry-season
260 abstraction (Shamsudduha et al., 2009; Shamsudduha et al., 2012) and high storage of the
261 regional unconsolidated sand aquifer, represented by a bulk specific yield (S_y) of 10% (Fig.
262 S38a). Time-series of GRACE and LSMs are shown in Fig. S39. The ensemble mean time
263 series of computed GRACE Δ GWS from three GRACE TWS solutions and five NASA
264 GLDAS LSMs is strongly correlated ($r = 0.86$, p value <0.001) to in situ Δ GWS derived



265 from a network of 236 piezometers (mean density of 1 piezometer per 610 km²) for the
266 period of 2003 to 2014. In the semi-arid Limpopo Basin where mean annual rainfall (469 mm
267 for the period of 2003 to 2015) is one-fifth of that in the Bengal Basin (2,276 mm), the
268 seasonal signal in Δ GWS, primarily in weathered crystalline rocks with a bulk S_y of 2.5%, is
269 smaller (Fig. S38b). Time-series of GRACE and LSMs are shown in Fig. S40. Comparison of
270 in situ Δ GWS, derived from a network of 40 piezometers (mean density of 1 piezometer per
271 1,175 km²), and computed GRACE-derived Δ GWS shows broad correspondence ($r = 0.62$, p
272 value < 0.001) though GRACE-derived Δ GWS is ‘noisier’; intra-annual variability may result
273 from uncertainty in the representation of other terrestrial stores using LSMs that are used to
274 compute GRACE-derived Δ GWS from GRACE Δ TWS. The magnitude of uncertainty in
275 monthly Δ SWs, Δ SMS, and Δ SNS that are estimated by GLDAS LSMs to compute
276 GRACE-derived Δ GWS in each large-scale aquifer system, is depicted in Fig. 2 and
277 supplementary Figs. S1-S36. The favourable, statistically significant correlations between the
278 computed ensemble mean GRACE-derived Δ GWS and in situ Δ GWS shown in these two
279 contrasting basins indicate that, at large scales ($\sim 200,000$ km²), the methodology used to
280 compute GRACE-derived Δ GWS has merit.

281 3.3 Trends in GRACE- Δ GWS time series

282 Computation of GRACE-derived Δ GWS for the 37 large-scale aquifers globally is shown in
283 Figs. 2 and 5. Figure 2 shows the ensemble GRACE Δ TWS and GLDAS LSM datasets used
284 to compute GRACE-derived Δ GWS for the High Plains Aquifer System in the USA (aquifer
285 no. 17 in Fig. 1); datasets used for all other large-scale aquifer systems are given in the
286 Supplementary Material (Figs. S1–S36). In addition to the ensemble mean, we show
287 uncertainty in GRACE-derived Δ GWS associated with 20 potential realisations from
288 GRACE products and LSMs. Monthly time-series data of ensemble GRACE-derived Δ GWS
289 for the other 36 large-scale aquifers are plotted (absolute scale) in Fig. 5 (in black) and fitted



290 with a Loess-based trend (in blue). For all but five large aquifer systems (e.g., Lake Chad
291 Basin-WHYMAP no. 7, Umm Ruwaba-8, Amazon-19, West Siberian Basin-25, and East
292 European-33), the dominant time-series component explaining variance in GRACE-derived
293 Δ GWS is trend (Fig. 3b, and supplementary Figs. S41-S77). Trends in GRACE-derived
294 Δ GWS are, however, overwhelmingly non-linear (curvilinear); linear trends adequately (R^2
295 >0.5 , p value <0.05) explain variability in GRACE-derived Δ GWS in just 5 of 37 large-scale
296 aquifer systems and of these, only two (Arabian-22, Canning-37) are declining. GRACE-
297 derived Δ GWS for three intensively developed, large-scale aquifer systems (Supplementary
298 Table S1: California Central Valley-16, Ganges-Brahmaputra-24, North China Plains-29)
299 show episodic declines (Fig. 5) though, in each case, their overall trend from 2002 to 2016 is
300 non-linear (Fig. 1).

301 **3.4 Computational uncertainty in GRACE- Δ GWS**

302 For several large aquifer systems primarily in arid and semi-arid environments, we identify
303 anomalously negative or positive estimates of GRACE-derived Δ GWS that deviate
304 substantially from underlying trends (Fig. 6 and supplementary Fig. S78). For example, the
305 semi-arid Upper Kalahari-Cuvelai-Zambezi Basin (11) features an extreme, negative anomaly
306 in GRACE-derived Δ GWS (Fig. 6a) in 2007-08 that is the consequence of simulated values
307 of terrestrial stores (Δ SWS + Δ SMS) by GLDAS LSMs that exceed the ensemble GRACE
308 Δ TWS signal. Inspection of individual time-series data for this basin (Fig. S11) reveals
309 greater consistency in the three GRACE- Δ TWS time-series data (variance of CSR: 111 cm²;
310 Mascons: 164 cm²; GRGS: 169 cm²) compared to simulated Δ SMS among the 4 GLDAS
311 LSMs (variance of CLM: 9 cm²; Mosaic: 90 cm²; Noah: 98 cm²; VIC is 110 cm²). In the
312 humid Congo Basin (10), positive Δ TWS values in 2006-07 but negative Δ SMS values
313 produce anomalously high values of GRACE-derived Δ GWS (Fig. 6b, Fig. S10). In the
314 snow-dominated, humid Angara-Lena Basin (27), a strongly positive, combined signal of



315 Δ SNS + Δ SWS exceeding Δ TWS leads to a very negative estimation of Δ GWS when
316 groundwater is following a rising trend (Fig. 6c, Fig. S26).

317 **3.5 GRACE Δ GWS and extreme precipitation**

318 Non-linear trends in GRACE-derived Δ GWS (i.e. difference in STL trend component
319 between two consecutive years) demonstrate a significant association with precipitation
320 anomalies from CRU dataset for each hydrological year (i.e. percent deviations from mean
321 annual precipitation between 2002 and 2016) in semi-arid environments (Fig. 7, Pearson
322 correlation, $r=0.62$, $p<0.001$). These associations over extreme hydrological years are
323 particularly strong in a number of individual aquifer systems (Fig. 5; Supplementary Tables
324 S3 and S4) including the Great Artesian Basin (36) ($r=0.93$), California Central Valley (16)
325 ($r=0.88$), North Caucasus Basin (34) ($r=0.65$), Umm Ruwaba Basin (8) ($r=0.64$), and
326 Ogallala (High Plains) Aquifer (17) ($r=0.64$). In arid aquifer systems, overall associations
327 between GRACE Δ GWS and precipitation anomalies are statistically significant but
328 moderate ($r=0.36$, $p<0.001$); a strong association is found only for the Canning Basin (37)
329 ($r=0.52$). In humid (and sub-humid) aquifer systems, no overall statistically significant
330 association is found yet strong correlations are noted for two temperate aquifer systems
331 (Northern Great Plains Aquifer (14), $r=0.51$; Angara–Lena Basin (27), $r=0.54$); weak
332 correlations are observed in the humid tropics for the Maranhao Basin (20, $r=0.24$) and
333 Ganges-Brahmaputra Basin (24, $r=0.28$).

334 Distinct rises observed in GRACE-derived Δ GWS correspond with extreme seasonal
335 (annual) precipitation (Fig. 5; Table S3 and Table S4). In the semi-arid Great Artesian Basin
336 (aquifer no. 36) (Fig. 5 and supplementary Fig. S35), two consecutive years (2009–10 and
337 2010–11) of statistically extreme (i.e., $>90^{\text{th}}$ percentile, period: 1901 to 2016) precipitation
338 interrupt a multi-annual (2002 to 2009) declining trend. Pronounced rises in GRACE-derived



339 Δ GWS in response to extreme annual rainfall are visible in other semi-arid, large aquifer
340 systems including the Umm Ruwaba Basin (8) in 2007, Lower Kalahari-Stampriet Basin (12)
341 in 2011, California Central Valley (16) in 2005, Ogallala (High Plains) Aquifer (17) in 2015,
342 and Indus Basin (23) in 2010 and 2015 (Tables S3 and S4 and Figs. S2, S8, S12, S16, S22).
343 Similar rises in GRACE-derived Δ GWS in response to extreme annual rainfall in arid basins
344 include the Lake Chad Basin (7) in 2012 and Ogaden-Juba Basin (9) in 2013 (Table S3 and
345 Figs. S7, S9). In the Canning Basin, a substantial rise in GRACE-derived Δ GWS occurs in
346 2010-11 (Tables S3 and S4 and Fig. S36) in response to extreme annual rainfall though the
347 overall trend is declining.

348 Non-linear trends that feature substantial rises in GRACE-derived Δ GWS in response to
349 extreme annual precipitation under humid climates, are observed in the Maranhao Basin (20)
350 in 2008-09, Guarani Aquifer System (21) in 2015-16, and North China Plains (29) in 2003.
351 Consecutive years of extreme precipitation in 2012 and 2013 also generate a distinct rise in
352 GRACE-derived Δ GWS in the Song-Liao Plain (30) (Tables S3 and S4 and Figs. S29). In the
353 heavily developed (Table S2) Ganges-Brahmaputra Basin (24), a multi-annual (2002 to 2010)
354 declining trend is halted by an extreme (i.e. highest over the GRACE period of 2002 to 2016
355 but 59th percentile over the period of 1901 to 2016 using CRU dataset) annual precipitation in
356 2011 (Tables S3 and S4 and Figs. S23). Consecutive years from 2014 to 2015 of extreme
357 annual precipitation increase GRACE-derived Δ GWS and disrupt a multi-annual declining
358 trend in the West Siberian Artesian Basin (25) (Tables S3 and S4 and Figs. S24). In the sub-
359 humid Northern Great Plains (14), distinct rises in GRACE-derived Δ GWS occur in 2010
360 (Tables S3 and S4 and Figs. S14) in response to extreme annual precipitation though the
361 overall trend is linear and rising. The overall agreement in mean annual precipitation between
362 the CRU and GPCP datasets for the period of 1901 to 2016 is strong (median correlation
363 coefficient in 37 aquifer systems, $r=0.92$).



364 **4 Discussion**

365 **4.1 Uncertainty in GRACE-derived Δ GWS**

366 We compute a range of uncertainty in GRACE-derived Δ GWS associated with 20 potential
367 realisations from various GRACE (CSR, JPL-Mascons, GRGS) products and LSMs (CLM,
368 Noah, VIC, Mosaic). Uncertainty is generally higher for aquifers systems located in arid to
369 hyper-arid environments (Table 2, see supplementary Fig. S79). Computation of GRACE-
370 derived Δ GWS relies upon uncalibrated simulations of individual terrestrial water stores (i.e.,
371 Δ SWS, Δ SWS, Δ SNS) from LSMs to estimate Δ GWS from GRACE Δ TWS. A recent
372 global-scale comparison of Δ TWS estimated by GLDAS LSMs and GRACE (Scanlon et al.,
373 2018) indicates that LSMs systematically underestimate water storage changes. Here, we
374 detect probable errors in GLDAS LSM data from events that produce large deviations in
375 GWS (Fig. 5). These errors occur because GRACE-derived Δ GWS is computed as residual
376 (equation 1); overestimation (or underestimation) of these combined stores produces negative
377 (or positive) values of GRACE-derived Δ GWS when the aggregated value of other terrestrial
378 water stores is strongly positive (or negative) and no lag is assumed. It remains, however,
379 unclear whether overestimation of GWS from GRACE occurs systematically from the
380 common underestimation of terrestrial water stores identified by Scanlon et al. (2018).
381 Evidence from limited piezometric data presented here and elsewhere (Panda and Wahr,
382 2015; Feng et al., 2018) suggests that the dynamics in GRACE-derived Δ GWS are reasonable
383 yet the amplitude in Δ GWS from piezometry is scalable due to uncertainty in the applied S_y
384 (Shamsudduha et al., 2012).

385 Assessments of Δ GWS derived from GRACE are constrained in both limited timespan (last
386 15 years) and coarse spatial resolution ($>200,000$ km²). For example, centennial-scale
387 piezometry in the Ganges-Brahmaputra aquifer system (no. 24) reveals that recent



388 groundwater depletion in NW India traced by GRACE (Fig. 5 and supplementary Fig. S23)
389 (Rodell et al., 2009; Chen et al., 2014) follows more than a century of groundwater
390 accumulation through leakage of surface water via a canal network constructed primarily
391 during the 19th century (MacDonald et al., 2016). Long-term piezometric records from central
392 Tanzania and the Limpopo Basin of South Africa (Supplementary Fig. S80) show dramatic
393 increases in Δ GWS associated with extreme seasonal rainfall events that occurred prior to
394 2002 and thus provide a vital context to the more recent period of Δ GWS estimated by
395 GRACE. At regional scales, GRACE-derived Δ GWS can differ substantially from more
396 localised, in situ observations of Δ GWS from piezometry. In the Karoo Basin (aquifer no.
397 13), GRACE-derived Δ GWS is also rising (Fig. 5 and supplementary Fig. S13) over periods
398 during which groundwater depletion has been reported in parts of the basin (Rosewarne et al.,
399 2013). In the Guarani Aquifer System (21), groundwater depletion is reported from 2005 to
400 2009 in Ribeiro Preto near Sao Paulo as a result of intensive groundwater withdrawals for
401 urban water supplies and irrigation of sugarcane (Foster et al., 2009) yet GRACE-derived
402 Δ GWS over this same period is rising.

403 **4.2 Variability in GRACE Δ GWS and role of extreme precipitation**

404 Non-linear trends in GRACE-derived Δ GWS arise, in part, from inter-annual variability in
405 precipitation which has similarly been observed in analyses of GRACE Δ TWS (Humphrey et
406 al., 2016; Sun et al., 2017; Bonsor et al., 2018). Annual precipitation in the Great Artesian
407 Basin (aquifer no. 36) provides a dramatic example of how years (2009–10, 2010–11 from
408 both CRU and GPCC datasets) of extreme precipitation can generate anomalously high
409 groundwater recharge that arrests a multi-annual declining trend (Fig. 5), increasing
410 variability in GRACE-derived Δ GWS over the relatively short period (15 years) of GRACE
411 data. The disproportionate contribution of episodic, extreme rainfall to groundwater recharge
412 has previously been shown by (Taylor et al., 2013b) from long-term piezometry in semi-arid



413 central Tanzania where nearly 20% of the recharge observed over a 55-year period resulted
414 from a single season of extreme rainfall, associated with the strongest El Niño event (1997–
415 1998) of the last century (Supplementary Fig. S80a). Further analysis from multi-decadal
416 piezometric records in drylands across tropical Africa (Cuthbert et al., 2019) confirm this bias
417 in response to intensive precipitation.

418 The dependence of groundwater replenishment on extreme annual precipitation indicated by
419 GRACE-derived ΔGWS for many of the world's large aquifer systems is consistent with
420 evidence from other sources. In a pan-tropical comparison of stable-isotope ratios of oxygen
421 ($^{18}\text{O}:^{16}\text{O}$) and hydrogen ($^2\text{H}:^1\text{H}$) in rainfall and groundwater, Jasechko and Taylor (2015)
422 show that recharge is biased to intensive monthly rainfall, commonly exceeding the 70th
423 percentile. In humid Uganda, Owor et al. (2009) demonstrate that groundwater recharge
424 observed from piezometry is more strongly correlated to daily rainfall exceeding a threshold
425 (10 mm) than all daily rainfalls. Periodicity in groundwater storage indicated by both
426 GRACE and in situ data has been associated with large-scale synoptic controls on
427 precipitation (e.g., El Niño Southern Oscillation, Pacific Decadal Oscillation,) in southern
428 Africa (Kolusu et al., 2019), and have been shown to amplify recharge in major US aquifers
429 (Kuss and Gurdak, 2014) and groundwater depletion in India (Mishra et al., 2016). There are,
430 however, large-scale aquifer systems where GRACE-derived ΔGWS exhibits comparatively
431 weak correlations to precipitation. In the semi-arid Iullemeden-Irhazer Aquifer (6) variance
432 in rainfall over the period of GRACE observation following the multi-decadal Sahelian
433 drought is low (Table S1) and the net rise in GRACE-derived ΔGWS is associated with
434 changes in the terrestrial water balance associated with land-cover change (Ibrahim et al.,
435 2014).



436 Our analysis identifies non-linear trends in GRACE-derived Δ GWS for the vast majority (32
437 of 37) of the world's large aquifer systems (Figs. 1, 5 and 8). Non-linearity reflects, in part,
438 the variable nature of groundwater replenishment observed at the scale of the GRACE
439 footprint that is consistent with more localised, emerging evidence from multi-decadal
440 piezometric records (Taylor et al., 2013b) (Supplementary Fig. S80). The variable and often
441 episodic nature of groundwater replenishment complicates assessments of the sustainability
442 of groundwater withdrawals and highlights the importance of long-term observations over
443 decadal timescales in undertaking such evaluations. An added complication to evaluations of
444 the sustainability of groundwater withdrawals under climate change is uncertainty in how
445 radiative forcing will affect large-scale controls on regional precipitation like El Niño
446 Southern Oscillation (Latif and Keenlyside, 2009). The developed set of GRACE-derived
447 Δ GWS time series data for the world's large aquifer systems provided here offers a
448 consistent, additional benchmark alongside long-term piezometry to assess not only large-
449 scale climate controls on groundwater replenishment but also opportunities to enhance
450 groundwater storage through managed aquifer recharge.

451

452 **5 Conclusions**

453 Changes in groundwater storage (Δ GWS) computed from GRACE satellite data continue to
454 rely upon uncertain, uncalibrated estimates of changes in other terrestrial stores of water
455 found in soil, surface water, and snow/ice from global-scale models. The application here of
456 ensemble mean values of three GRACE Δ TWS processing strategies (CSR, JPL-Mascons,
457 GRGS) and five land-surface models (GLDAS 1: CLM, Noah, VIC, Mosaic; GLDAS 2:
458 Noah) is designed to reduce the impact of uncertainty in an individual model or GRACE
459 product on the computation of GRACE-derived Δ GWS. We, nevertheless, identify a few



460 instances where erroneously high or low values of GRACE-derived Δ GWS are computed;
461 these occur primarily in arid and semi-arid environments where uncertainty in the simulation
462 of terrestrial water balances is greatest. Over the period of GRACE observation (2002 to
463 2016), we show favourable comparisons between GRACE-derived Δ GWS and piezometric
464 observations ($r = 0.62$ to 0.86) in two contrasting basins (i.e. semi-arid Limpopo Basin,
465 tropical humid Bengal Basin) for which in situ data are available. This study thus contributes
466 to a growing body of research and observations reconciling computed GRACE-derived
467 Δ GWS to ground-based data.

468 GRACE-derived Δ GWS from 2002 to 2016 for the world's 37 large-scale aquifer systems
469 shows substantial variability as revealed explicitly by 20 potential realisations from GRACE
470 products and LSMs computed here; trends in ensemble mean GRACE-derived Δ GWS are
471 overwhelmingly (87%) non-linear (Fig. 8). Linear trends adequately explain variability in
472 GRACE-derived Δ GWS in just 5 aquifer systems for which linear declining trends, indicative
473 of groundwater depletion, are observed in 2 aquifer systems. This non-linearity in GRACE-
474 derived Δ GWS for the vast majority of the world's large aquifer systems is inconsistent with
475 narratives of global-scale groundwater depletion. Groundwater depletion, more commonly
476 observed by piezometry, is experienced at scales well below the GRACE footprint ($<200,000$
477 km^2) and likely to be more pervasive than suggested by the presented analysis of large-scale
478 aquifers. Non-linearity in GRACE-derived Δ GWS arises, in part, from episodic recharge
479 associated with extreme ($>90^{\text{th}}$ percentile) annual precipitation. This episodic replenishment
480 or recharge of groundwater, combined with natural discharges that sustain ecosystem
481 functions and human withdrawals, produces highly dynamic aquifer systems that complicate
482 assessments of the sustainability of large aquifer systems. These findings also highlight
483 potential opportunities for sustaining groundwater withdrawals through induced recharge
484 from extreme precipitation and managed aquifer recharge.



485 **References**

- 486 Asoka, A., Gleeson, T., Wada, Y., and Mishra, V.: Relative contribution of monsoon
487 precipitation and pumping to changes in groundwater storage in India, *Nature Geosci.*,
488 10, 109-117, 2017.
- 489 Bhanja, S. N., Mukherjee, A., Saha, D., Velicogna, I., and Famiglietti, J. S.: Validation of
490 GRACE based groundwater storage anomaly using in-situ groundwater level
491 measurements in India, *Journal of Hydrology*, 543, 729-738, 2016.
- 492 Biancale, R., Lemoine, J.-M., Balmino, G., Loyer, S., Bruisma, S., Perosanz, F., Marty, J.-C.,
493 and Gégout, P.: 3 Years of Geoid Variations from GRACE and LAGEOS Data at 10-day
494 Intervals from July 2002 to March 2005, CNES/GRGS, 2006.
- 495 Bonsor, H. C., Shamsudduha, M., Marchant, B. P., MacDonald, A. M., and Taylor, R. G.:
496 Seasonal and Decadal Groundwater Changes in African Sedimentary Aquifers Estimated
497 Using GRACE Products and LSMs, *Remote Sensing*, 10, 2018.
- 498 Castellazzi, P., Martel, R., Rivera, A., Huang, J., Pavlic, G., Calderhead, A. I., Chaussard, E.,
499 Garfias, J., and Salas, J.: Groundwater depletion in Central Mexico: Use of GRACE and
500 InSAR to support water resources management, *Water Resour. Res.*, 52, 5985-6003,
501 doi:10.1002/2015WR018211, 2016.
- 502 Chatfield, C.: *The analysis of time series - an introduction*, 6th ed., Chapman and Hall, CRC
503 Press, Boca Raton, 2003.
- 504 Chen, J., Li, J., Zhang, Z., and Ni, S.: Long-term groundwater variations in Northwest India
505 from satellite gravity measurements, *Global and Planetary Change*, 116, 130-138, 2014.
- 506 Cleveland, R. B., Cleveland, W. S., McRae, J. E., and Terpenning, I.: STL: A Seasonal Trend
507 Decomposition Procedure Based on LOESS, *J. Official Statistics*, 6, 3-33, 1990.
- 508 Cuthbert, M. O., Taylor, R. G., Favreau, G., Todd, M. C., Shamsudduha, M., Villholth, K. G.,
509 MacDonald, A. M., Scanlon, B. R., Kotchoni, D. O. V., Vouillamoz, J.-M., Lawson, F.
510 M. A., Adjomayi, P. A., Kashaigili, J., Seddon, D., Sorensen, J. P. R., Ebrahim, G. Y.,
511 Owor, M., Nyenje, P. M., Nazoumou, Y., Goni, I., Ousmane, B. I., Sibanda, T., Ascott,
512 M. J., Macdonald, D. M. J., Agyekum, W., Koussoubé, Y., Wanke, H., Kim, H., Wada,
513 Y., Lo, M.-H., Oki, T., and Kukuric, N.: Observed controls on resilience of groundwater
514 to climate variability in sub-Saharan Africa, *Nature*, 572, 230-234,
515 <https://doi.org/10.1038/s41586-019-1441-7>, 2019.
- 516 Dai, Y., Zeng, X., Dickinson, R. E., Baker, I., Bonan, G. B., Bosilovich, M. G., Denning, A.
517 S., Dirmeyer, P. A., Houser, P. R., Niu, G., Oleson, K. W., Schlosser, C. A., and Yang,
518 Z.-L.: The common land model (CLM), *Bull. Am. Meteorol. Soc.*, 84, 1013-1023, 2003.
- 519 Döll, P., Hoffmann-Dobrev, H., Portmann, F. T., Siebert, S., Eicker, A., Rodell, M.,
520 Strassberg, G., and Scanlon, B. R.: Impact of water withdrawals from groundwater and
521 surface water on continental water storage variations, *Journal of Geodynamics*, 59-60,
522 143-156, 2012.



- 523 Döll, P., Schmied, H. M., Schuh, C., Portmann, F. T., and Eicker, A.: Global-scale
524 assessment of groundwater depletion and related groundwater abstractions: Combining
525 hydrological modeling with information from well observations and GRACE satellites,
526 *Water Resour. Res.*, 50, 5698-5720, doi:10.1002/2014WR015595, 2014.
- 527 Ek, M. B., Mitchell, K. E., Lin, Y., Rogers, E., Grunmann, P., Koren, V., Gayno, G., and
528 Tarpley, J. D.: Implementation of Noah land surface model advances in the National
529 Centers for Environmental Prediction operational mesoscale Eta model, *J. Geophys.*
530 *Res.*, 108(D22), 8851, 10.1029/2002JD003296, 2003.
- 531 Famiglietti, J. S., Lo, M., Ho, S. L., Bethune, J., Anderson, K. J., Syed, T. H., Swenson, S.
532 C., Linage, C. R. d., and Rodell, M.: Satellites measure recent rates of groundwater
533 depletion in California's Central Valley, *Geophys. Res. Lett.*, 38, L03403,
534 10.1029/2010GL046442, 2011.
- 535 Famiglietti, J. S., and Rodell, M.: Water in the Balance, *Science*, 340, 1300-1301,
536 doi:10.1126/science.1236460, 2013.
- 537 Famiglietti, J. S.: The global groundwater crisis, *Nature Climate Change*, 4, 945-948,
538 doi:10.1038/nclimate2425, 2014.
- 539 Feng, W., Shum, C. K., Zhong, M., and Pan, Y.: Groundwater Storage Changes in China
540 from Satellite Gravity: An Overview, *Remote Sensing*, 10, 674, 2018.
- 541 Foster, S., Hirata, R., Vidal, A., Schmidt, G., and Garduño, H.: The Guarani Aquifer
542 Initiative - Towards Realistic Groundwater Management in a Transboundary Context,
543 *The World Bank*, Washington D.C., 28, 2009.
- 544 Getirana, A., Kumar, S., Giroto, M., and Rodell, M.: Rivers and Floodplains as Key
545 Components of Global Terrestrial Water Storage Variability, *Geophysical Research*
546 *Letters*, 44, 10359-10368, 2017.
- 547 Harris, I., Jones, P. D., Osborn, T. J., and Lister, D. H.: Updated high-resolution grids of
548 monthly climatic observations - the CRU TS3.10 Dataset, *International Journal of*
549 *Climatology*, 34, 623-642, 2014.
- 550 Hassan, A. A., and Jin, S.: Lake level change and total water discharge in East Africa Rift
551 Valley from satellite-based observations, *Global Planet Change*, 117, 79-90,
552 10.1016/j.gloplacha.2014.03.005, 2014.
- 553 Humphrey, V., Gudmundsson, L., and Seneviratne, S. I.: Assessing Global Water Storage
554 Variability from GRACE: Trends, Seasonal Cycle, Subseasonal Anomalies and
555 Extremes, *Surveys in Geophysics*, 37, 357-395, doi:10.1007/s10712-016-9367-1, 2016.
- 556 Ibrahim, M., Favreau, G., Scanlon, B. R., Seidel, J. L., Coz, M. L., Demarty, J., and
557 Cappelaere, B.: Long-term increase in diffuse groundwater recharge following expansion
558 of rainfed cultivation in the Sahel, West Africa, *Hydrogeol. J.*, 22, 1293-1305, 2014.
- 559 Jacoby, W. G.: Loess::a nonparametric, graphical tool for depicting relationships between
560 variables, *Electoral Studies*, 19, 577-613, 2000.



- 561 Jasechko, S., and Taylor, R. G.: Intensive rainfall recharges tropical groundwaters,
562 *Environmental Research Letters*, 10, 124015, 2015.
- 563 Kim, H., Yeh, P. J.-F., Oki, T., and Kanae, S.: Role of rivers in the seasonal variations of
564 terrestrial water storage over global basins, *Geophys. Res. Lett.*, 36, L17402,
565 doi:10.1029/2009GL039006, 2009.
- 566 Kolusu, S. R., Shamsudduha, M., Todd, M. C., Taylor, R. G., Seddon, D., Kashaigili, J. J.,
567 Girma, E., Cuthbert, M., Sorensen, J. P. R., Villholth, K. G., MacDonald, A. M., and
568 MacLeod, D. A.: The El Niño event of 2015-16: Climate anomalies and their impact on
569 groundwater resources in East and Southern Africa, *Hydrol. Earth Syst. Sci.*, 23, 1751-
570 1762, 2019.
- 571 Koster, R. D., and Suarez, M. J.: Modeling the land surface boundary in climate models as a
572 composite of independent vegetation stands, *J. Geophys. Res.*, 97, 2697-2715, 1992.
- 573 Kumar, S. V., Peters-Lidard, C. D., Tian, Y., Houser, P. R., Geiger, J., Olden, S., Lighty, L.,
574 Eastman, J. L., Doty, B., Dirmeyer, P., Adams, J., Mitchell, K., Wood, E. F., and
575 Sheffield, J.: Land information system: An interoperable framework for high resolution
576 land surface modeling, *Environmental Modelling & Software*, 21, 1402-1415, 2006.
- 577 Kuss, A. J. M., and Gurdak, J. J.: Groundwater level response in U.S. principal aquifers to
578 ENSO, NAO, PDO, and AMO, *Journal of Hydrology*, 519 (Part B), 1939-1952, 2014.
- 579 Landerer, F. W., and Swenson, S. C.: Accuracy of scaled GRACE terrestrial water storage
580 estimates, *Water Resour. Res.*, 48, W04531, 2012.
- 581 Latif, M., and Keenlyside, N. S.: El Niño/Southern Oscillation response to global warming,
582 *Proceedings of the National Academy of Sciences*, 106, 20578-20583,
583 doi:10.1073/pnas.0710860105, 2009.
- 584 Liang, X., Xie, Z., and Huang, M.: A new parameterization for surface and groundwater
585 interactions and its impact on water budgets with the variable infiltration capacity (VIC)
586 land surface model, *J. Geophys. Res.*, 108(D16), 8613, 10.1029/2002JD003090, 2003.
- 587 Longuevergne, L., Wilson, C. R., Scanlon, B. R., and Crétaux, J. F.: GRACE water storage
588 estimates for the Middle East and other regions with significant reservoir and lake
589 storage, *Hydrol. Earth Syst. Sci.*, 17, 4817-4830, doi:10.5194/hess-17-4817-2013, 2013.
- 590 MacDonald, A. M., Bonsor, H. C., Ahmed, K. M., Burgess, W. G., Basharat, M., Calow, R.
591 C., Dixit, A., Foster, S. S. D., Gopal, K., Lapworth, D. J., Lark, R. M., Moench, M.,
592 Mukherjee, A., Rao, M. S., Shamsudduha, M., Smith, L., Taylor, R. G., Tucker, J., van
593 Steenberg, F., and Yadav, S. K.: Groundwater quality and depletion in the Indo-
594 Gangetic Basin mapped from in situ observations, *Nature Geosci.*, 9, 762-766, 2016.
- 595 Mishra, V., Aadhar, S., Asoka, A., S. Pai, and Kumar, R.: On the frequency of the 2015
596 monsoon season drought in the Indo-Gangetic Plain, *Geophys. Res. Lett.*, 43, 12102-
597 12112, 10.1002/GL071407, 2016.
- 598 Owor, M., Taylor, R. G., Tindimugaya, C., and Mwesigwa, D.: Rainfall intensity and
599 groundwater recharge: empirical evidence from the Upper Nile Basin, *Environmental
600 Research Letters*, 1-6, 2009.



- 601 Panda, D. K., and Wahr, J.: Spatiotemporal evolution of water storage changes in India from
602 the updated GRACE-derived gravity records, *Water Resour. Res.*, 51, 135–149,
603 doi:10.1002/2015WR017797, 2015.
- 604 Richey, A. S., Thomas, B. F., Lo, M.-H., Reager, J. T., Famiglietti, J. S., Voss, K., Swenson,
605 S., and Rodell, M.: Quantifying renewable groundwater stress with GRACE, *Water*
606 *Resour. Res.*, 51, 5217-5238, doi:10.1002/2015WR017349, 2015.
- 607 Richts, A., Struckmeier, W. F., and Zaepke, M.: WHYMAP and the Groundwater Resources
608 of the World 1:25,000,000, in: *Sustaining Groundwater Resources. International Year of*
609 *Planet Earth*, edited by: J., J., Springer, Dordrecht, 159-173, 2011.
- 610 Rodell, M., Houser, P. R., Jambor, U., Gottschalck, J., Mitchell, K., Meng, C.-J., Arsenault,
611 K., Cosgrove, B., Radakovich, J., Bosilovich, M., Entin, J. K., Walker, J. P., Lohmann,
612 D., and Toll, D.: The Global Land Data Assimilation System, *Bull. Am. Meteorol. Soc.*,
613 85, 381-394, 2004.
- 614 Rodell, M., Chen, J., Kato, H., Famiglietti, J. S., Nigro, J., and Wilson, C. R.: Estimating
615 ground water storage changes in the Mississippi River basin (USA) using GRACE,
616 *Hydrogeol. J.*, 15, 159-166, doi:10.1007/s10040-006-0103-7, 2007.
- 617 Rodell, M., Velicogna, I., and Famiglietti, J. S.: Satellite-based estimates of groundwater
618 depletion in India, *Nature*, 460, 999-1003, doi:10.1038/nature08238, 2009.
- 619 Rodell, M., Famiglietti, J. S., Wiese, D. N., Reager, J. T., Beaudoin, H. K., Landerer, F. W.,
620 and Lo, M. H.: Emerging trends in global freshwater availability, *Nature*, 557, 651-659,
621 doi:10.1038/s41586-018-0123-1, 2018.
- 622 Rosewarne, P. N., Woodford, A. C., O'Brien, R., Tonder, G. V., Esterhuysen, C., Goes, M.,
623 Talma, A. S., Tredoux, G., and Visser, D.: *Karoo Groundwater Atlas, Volume 2. Karoo*
624 *Groundwater Expert Group (KGEG), Ground Water Division, The Geological Society of*
625 *South Africa, Cape Town, South Africa, 1-35, 2013.*
- 626 Scanlon, B. R., Faunt, C. C., Longuevergne, L., Reedy, R. C., Alley, W. M., McGuire, V. L.,
627 and McMahon, P. B.: Groundwater depletion and sustainability of irrigation in the US
628 High Plains and Central Valley, *Proc. Natl. Acad. Sci. USA*, 109, 9320-9325, 2012a.
- 629 Scanlon, B. R., Longuevergne, L., and Long, D.: Ground referencing GRACE satellite
630 estimates of groundwater storage changes in the California Central Valley, USA, *Water*
631 *Resour. Res.*, 48, W04520, 2012b.
- 632 Scanlon, B. R., Zhang, Z., Save, H., Sun, A. Y., Müller Schmied, H., van Beek, L. P. H.,
633 Wiese, D. N., Wada, Y., Long, D., Reedy, R. C., Longuevergne, L., Döll, P., and
634 Bierkens, M. F. P.: Global models underestimate large decadal declining and rising water
635 storage trends relative to GRACE satellite data, *PNAS*, 115 1080-1089,
636 doi:10.1073/pnas.1704665115, 2018.
- 637 Schneider, U., Finger, P., Meyer-Christoffer, A., Rustemeier, E., Ziese, M., and Becker, A.:
638 Evaluating the Hydrological Cycle over Land Using the Newly-Corrected Precipitation
639 Climatology from the Global Precipitation Climatology Centre (GPCC), *Atmosphere*, 8,
640 52, 10.3390/atmos8030052, 2017.



- 641 Shamsudduha, M., Chandler, R. E., Taylor, R. G., and Ahmed, K. M.: Recent trends in
642 groundwater levels in a highly seasonal hydrological system: the Ganges-Brahmaputra-
643 Meghna Delta, *Hydrol. Earth Syst. Sci.*, 13, 2373-2385, doi:10.5194/hess-13-2373-2009,
644 2009.
- 645 Shamsudduha, M., Taylor, R. G., and Longuevergne, L.: Monitoring groundwater storage
646 changes in the highly seasonal humid tropics: validation of GRACE measurements in the
647 Bengal Basin, *Water Resour. Res.*, 48, W02508, doi:10.1029/2011WR010993, 2012.
- 648 Shamsudduha, M., Taylor, R. G., Jones, D., Longuevergne, L., Owor, M., and Tindimugaya,
649 C.: Recent changes in terrestrial water storage in the Upper Nile Basin: an evaluation of
650 commonly used gridded GRACE products, *Hydrol. Earth Syst. Sci.*, 21, 4533-4549,
651 2017.
- 652 Sheffield, J., Goteti, G., and Wood, E. F.: Development of a 50-year high-resolution global
653 dataset of meteorological forcings for land surface modeling, *Journal of Climate*, 19,
654 3088-3111, 2006.
- 655 Strassberg, G., Scanlon, B. R., and Chambers, D.: Evaluation of groundwater storage
656 monitoring with the GRACE satellite: Case study of the High Plains aquifer, central
657 United States, *Water Resour. Res.*, 45, W05410, 2009.
- 658 Sun, A. Y., Scanlon, B. R., AghaKouchak, A., and Zhang, Z.: Using GRACE Satellite
659 Gravimetry for Assessing Large-Scale Hydrologic Extremes, *Remote Sensing*, 9, 1287,
660 doi:10.3390/rs9121287, 2017.
- 661 Swenson, S., Yeh, P. J.-F., Wahr, J., and Famiglietti, J. S.: A comparison of terrestrial water
662 storage variations from GRACE with in situ measurements from Illinois, *Geophys. Res.*
663 *Let.*, 33, L16401, doi:10.1029/2006GL026962, 2006.
- 664 Swenson, S., Famiglietti, J., Basara, J., and Wahr, J.: Estimating profile soil moisture and
665 groundwater variations using GRACE and Oklahoma Mesonet soil moisture data, *Water*
666 *Resour. Res.*, 44, W01413, doi:10.1029/2007WR006057, 2008.
- 667 Tapley, B. D., Bettadpur, S., Ries, J. C., Thompson, P. F., and Watkins, M. M.: GRACE
668 measurements of mass variability in the Earth system, *Science*, 305, 503-505, 2004.
- 669 Taylor, R. G., Scanlon, B., Doll, P., Rodell, M., van Beek, R., Wada, Y., Longuevergne, L.,
670 Leblanc, M., Famiglietti, J. S., Edmunds, M., Konikow, L., Green, T. R., Chen, J.,
671 Taniguchi, M., Bierkens, M. F. P., MacDonald, A., Fan, Y., Maxwell, R. M., Yechieli,
672 Y., Gurdak, J. J., Allen, D. M., Shamsudduha, M., Hiscock, K., Yeh, P. J. F., Holman, I.,
673 and Treidel, H.: Ground water and climate change, *Nature Climate Change*, 3, 322-329,
674 doi:10.1038/nclimate1744, 2013a.
- 675 Taylor, R. G., Todd, M. C., Kongola, L., Maurice, L., Nahozya, E., Sanga, H., and
676 MacDonald, A.: Evidence of the dependence of groundwater resources on extreme
677 rainfall in East Africa, *Nature Climate Change*, 3, 374-378, doi:10.1038/nclimate1731,
678 2013b.
- 679 Thomas, B. F., Caineta, J., and Nanteza, J.: Global assessment of groundwater sustainability
680 based on storage anomalies, *Geophysical Research Letters*, 44, 11445-11455,
681 doi:10.1002/2017GL076005, 2017.



- 682 Watkins, M. M., Wiese, D. N., Yuan, D.-N., Boening, C., and Landerer, F. W.: Improved
683 methods for observing Earth's time variable mass distribution with GRACE using
684 spherical cap mascons, *J. Geophys. Res. Solid Earth*, 120, 2648–2671,
685 doi:10.1002/2014JB011547, 2015.
- 686 Wiese, D. N., Landerer, F. W., and Watkins, M. M.: Quantifying and reducing leakage errors
687 in the JPL RL05M GRACE mascon solution, *Water Resour. Res.*, 52, 7490-7502,
688 10.1002/2016WR019344, 2016.

689

690 **Acknowledgements**

691 M.S. and R.T. acknowledge support from NERC-ESRC-DFID UPGro '*GroFutures*' (Ref.
692 NE/M008932/1; www.grofutures.org); R.T. also acknowledges the support of a Royal
693 Society – Leverhulme Trust Senior Fellowship (Ref. LT170004).

694

695 **Data Availability**

696 Supplementary information is available for this paper as a single PDF file. Data generated
697 and used in this study can be made available upon request to the corresponding author.



698 **Tables and Figures**

699 **Table 1.** Identification number, name and general location of the world's 37 large aquifer
 700 systems as provided in the WHYMAP database (<https://www.whymap.org/>). Mean climatic
 701 condition of each of the 37 aquifer systems based on the aridity index is tabulated.

702

WHYMAP aquifer no.	WHYMAP Aquifer name	Continent	Climate zones based on Aridity index	WHYMAP aquifer no.	WHYMAP Aquifer name	Continent	Climate zones based on Aridity index
1	Nubian Sandstone Aquifer System	Africa	Hyper-arid	20	Maranhao Basin	South America	Humid
2	Northwestern Sahara Aquifer System	Africa	Arid	21	Guarani Aquifer System (Parana Basin)	South America	Humid
3	Murzuk-Djado Basin	Africa	Hyper-arid	22	Arabian Aquifer System	Asia	Arid
4	Taoudeni-Tanezrouft Basin	Africa	Hyper-arid	23	Indus River Basin	Asia	Semi-arid
5	Senegal-Mauritanian Basin	Africa	Semi-arid	24	Ganges-Brahmaputra Basin	Asia	Humid
6	Iullemeden-Irhazer Aquifer System	Africa	Arid	25	West Siberian Artesian Basin	Asia	Humid
7	Lake Chad Basin	Africa	Arid	26	Tunguss Basin	Asia	Humid
8	Umm Ruwaba Aquifer (Sudd Basin)	Africa	Semi-arid	27	Angara-Lena Basin	Asia	Humid
9	Ogaden-Juba Basin	Africa	Arid	28	Yakut Basin	Asia	Humid
10	Congo Basin	Africa	Humid	29	North China Plains Aquifer System	Asia	Humid
11	Upper Kalahari-Cuvelai-Zambezi Basin	Africa	Semi-arid	30	Song-Liao Plain	Asia	Humid
12	Lower Kalahari-Stampriet Basin	Africa	Arid	31	Tarim Basin	Asia	Arid
13	Karoo Basin	Africa	Semi-arid	32	Paris Basin	Europe	Humid
14	Northern Great Plains Aquifer	North America	Sub-humid	33	East European Aquifer System	Europe	Humid
15	Cambro-Ordovician Aquifer System	North America	Humid	34	North Caucasus Basin	Europe	Semi-arid
16	California Central Valley Aquifer System	North America	Semi-arid	35	Pechora Basin	Europe	Humid
17	Ogallala Aquifer (High Plains)	North America	Semi-arid	36	Great Artesian Basin	Australia	Semi-arid
18	Atlantic and Gulf Coastal Plains Aquifer	North America	Humid	37	Canning Basin	Australia	Arid
19	Amazon Basin	South America	Humid				

703



704 **Table 2.** Variability (expressed as standard deviation) in GRACE-derived estimates of GWS
 705 from 20 realisations (3 GRACE-TWS and an ensemble mean of TWS, and 4 LSMs and an
 706 ensemble mean of surface water and soil moisture storage, and a snow water storage) and
 707 their reported range of uncertainty (% deviation from the ensemble mean) in world's 37 large
 708 aquifer systems.

WHYMAP aquifer no.	WHYMAP Aquifer name	Std. deviation in GRACE-GWS (cm)	Range of uncertainty (%)	WHYMAP aquifer no.	WHYMAP Aquifer name	Std. deviation in GRACE-GWS (cm)	Range of uncertainty (%)
1	Nubian Sandstone Aquifer System	1.05	83	20	Maranhao Basin	5.68	136
2	Northwestern Sahara Aquifer System	1.29	121	21	Guarani Aquifer System (Parana Basin)	3.37	77
3	Murzuk-Djado Basin	1.17	189	22	Arabian Aquifer System	2.01	163
4	Taoudeni-Tanezrouft Basin	0.99	193	23	Indus River Basin	3	78
5	Senegal-Mauritanian Basin	3.23	96	24	Ganges-Brahmaputra Basin	9.84	58
6	Iullemmeden-Irhazer Aquifer System	1.52	116	25	West Siberian Artesian Basin	7.53	79
7	Lake Chad Basin	2.23	91	26	Tunguss Basin	7.4	103
8	Umm Ruwaba Aquifer (Sudd Basin)	4.95	113	27	Angara-Lena Basin	3.73	48
9	Ogaden-Juba Basin	1.52	57	28	Yakut Basin	4.15	83
10	Congo Basin	5.09	98	29	North China Plains Aquifer System	3.93	77
11	Upper Kalahari-Cuvelai-Zambezi Basin	10.03	36	30	Song-Liao Plain	2.63	62
12	Lower Kalahari-Stampriet Basin	1.76	106	31	Tarim Basin	1.37	219
13	Karoo Basin	3.06	74	32	Paris Basin	4.06	84
14	Northern Great Plains Aquifer	4.18	111	33	East European Aquifer System	5.91	75
15	Cambro-Ordovician Aquifer System	4.56	44	34	North Caucasus Basin	4.67	66
16	California Central Valley Aquifer System	9.73	55	35	Pechora Basin	8.55	94
17	Ogallala Aquifer (High Plains)	4.05	104	36	Great Artesian Basin	2.77	69
18	Atlantic and Gulf Coastal Plains Aquifer	2.56	193	37	Canning Basin	5.34	57
19	Amazon Basin	10.93	58				

709

710



711 **Main Figures:**

712

713

714

715

716

717

718

719

720

721

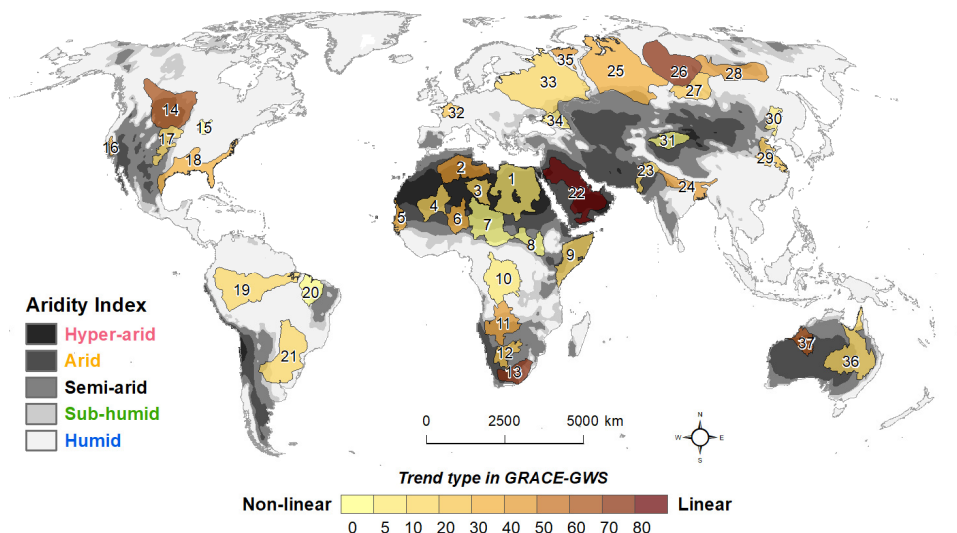
722

723

724

725

726



727 **Fig. 1.** Global map of 37 large aquifer systems from the GIS database of the World-wide
728 Hydrogeological Mapping and Assessment Programme (WHYMAP); names of these aquifer
729 systems are listed in Table 1 and correspond to numbers shown on this map for reference.
730 Grey shading shows the aridity index based on CGIAR's database of the Global Potential
731 Evapo-Transpiration (Global-PET) and Global Aridity Index (<https://cgiarcsi.community/>);
732 the proportion (as a percentage) of long-term trends in GRACE-derived Δ GWS of these large
733 aquifer systems that is explained by linear trend fitting is shown in colour (i.e. linear trends
734 toward red and non-linear trends toward blue).



735
736
737
738
739
740
741
742
743
744
745
746
747
748
749
750
751
752
753
754
755
756
757

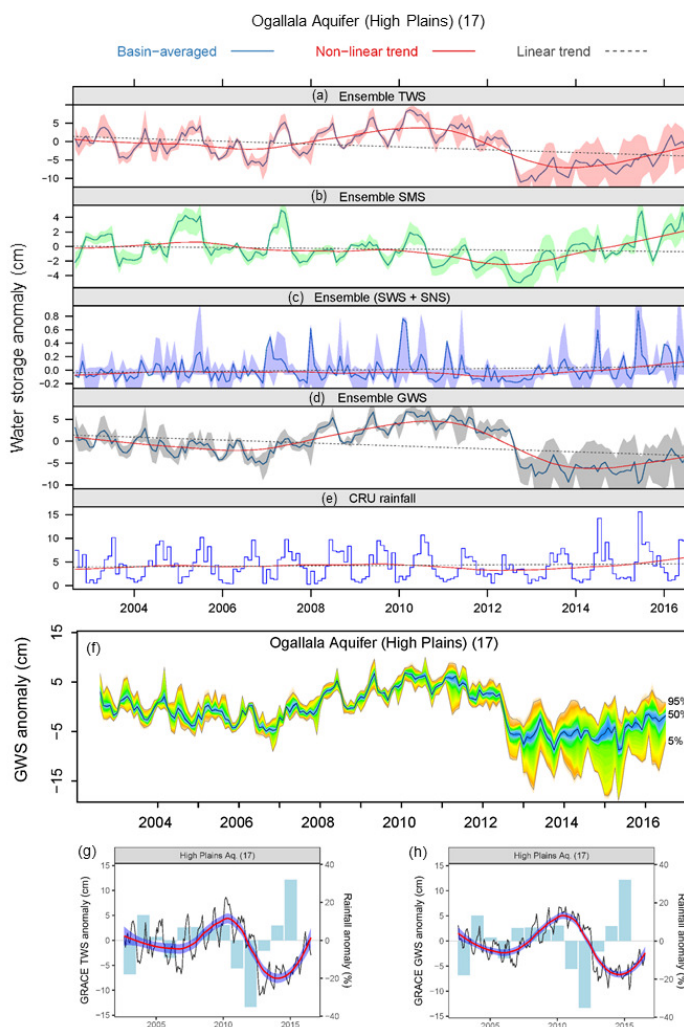


Fig. 2. Time-series data of terrestrial water storage anomaly (ΔTWS) from GRACE and individual water stores from GLDAS Land Surface Models (LSMs): (a) Ensemble monthly GRACE ΔTWS from three solutions (CSR, Mascons, GRGS), (b-c) ensemble monthly ΔSMS and $\Delta SWS + \Delta SNS$ from four GLDAS LSMs (CLM, Noah, VIC, Mosaic), (d) computed monthly ΔGWS and (e) monthly precipitation from August 2002 to July 2016, (f) range of uncertainty in GRACE-derived GWS from 20 realisations, (g) ensemble TWS and annual precipitation, and (h) ensemble GRACE-derived GWS and annual precipitation for the High Plains Aquifer System in the USA (WHYMAP aquifer no. 17). Values in the Y-axis of the top four panels show monthly water-storage anomalies (cm) and the bottom panel shows monthly precipitation (cm). Time-series data (a-e) for the 36 large aquifer systems can be found in supplementary Figs. S1-S36.



769

770

771

772

773

774

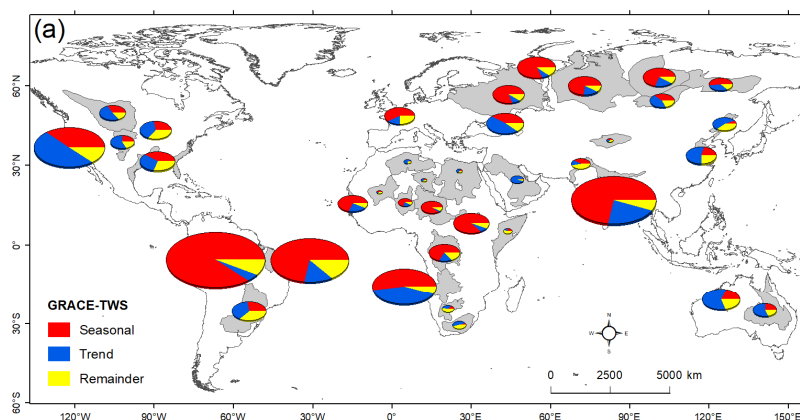
775

776

777

778

779



780

781

782

783

784

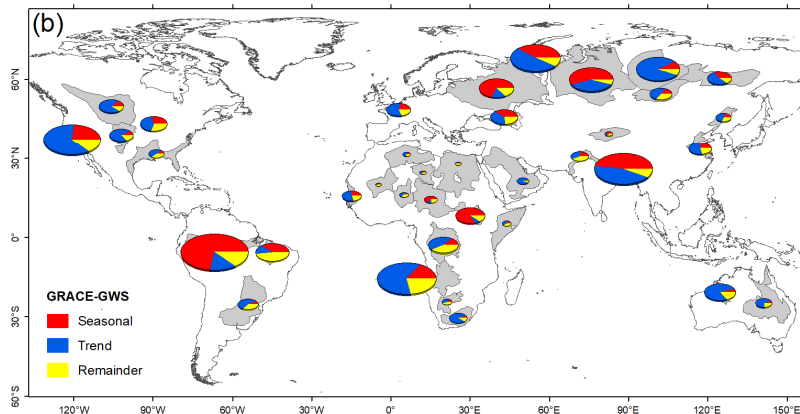
785

786

787

788

789



790

791

792

793

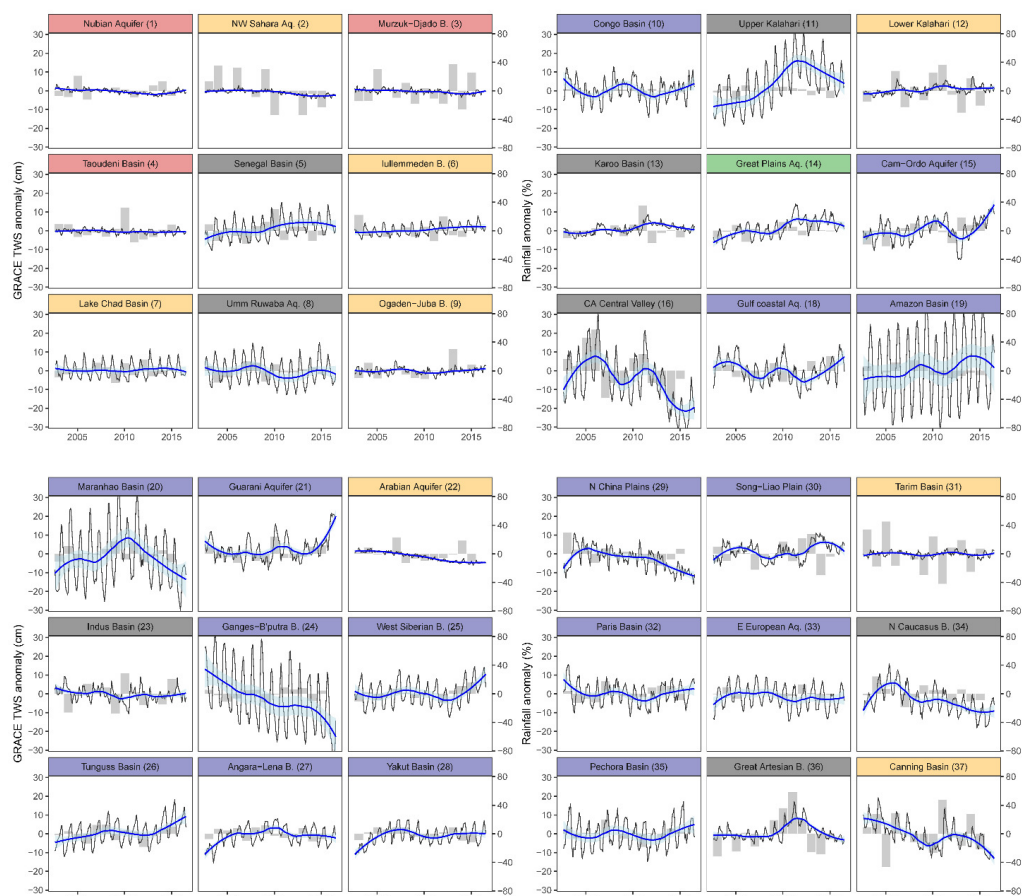
794

795

Fig. 3. Seasonal-Trend decomposition of (a) GRACE Δ TWS and (b) GRACE Δ GWS time-series data (2002 to 2016) for the world's 37 large aquifer systems using the STL decomposition method; seasonal, trend and remainder or irregular components of time-series data are decomposed and plotted as pie charts that are scaled by the variance of the time series in each aquifer system.



796



797

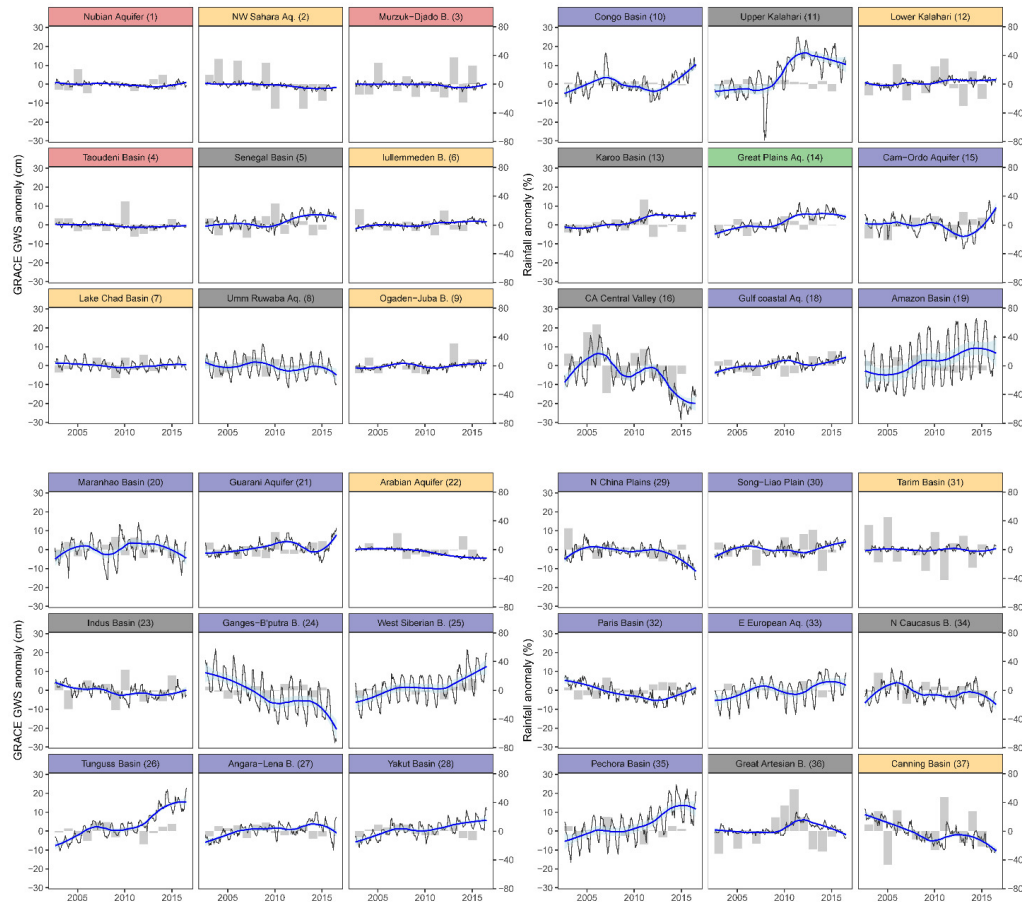
798

799 **Fig. 4.** Monthly time-series data (black) of ensemble GRACE Δ TWS for 36 large aquifer
800 systems with a fitted non-linear trend line (Loess smoothing line in thick blue) through the
801 time-series data; GRACE Δ TWS for the remaining large aquifer system (High Plains Aquifer
802 System, (WHYMAP aquifer no. 17) is given in Fig. 2. Shaded area in semi-transparent cyan
803 shows the range of 95% confidence interval of the fitted loess-based non-linear trends; light
804 grey coloured bar diagrams behind the lines on each panel show annual precipitation anomaly
805 (i.e. percentage deviation from the mean precipitation for the period of 1901 to 2016); banner
806 colours indicate the dominant climate of each aquifer based on the mean aridity index shown
807 in the legend on Fig. 1.

808



809



810

811

812 **Fig. 5.** Monthly time-series data (black) of ensemble GRACE Δ GWS for 36 large aquifer
813 systems with a fitted non-linear trend line (Loess smoothing line in thick blue) through the
814 time-series data; GRACE Δ GWS for the remaining large aquifer system (High Plains Aquifer
815 System, (WHYMAP aquifer no. 17) is given in Fig. 2. Shaded area in semi-transparent cyan
816 shows the range of 95% confidence interval of the fitted loess-based non-linear trends; light
817 grey coloured bar diagrams behind the lines on each panel show annual precipitation anomaly
818 (i.e. percentage deviation from the mean precipitation for the period of 1901 to 2016); banner
819 colours indicate the dominant climate of each aquifer based on the mean aridity index shown
820 in the legend on Fig. 1.

821

822



823

824

825

826

827

828

829

830

831

832

833

834

835

836

837

838

839

840

841

842

843

844

845

846

847

848

849

850

851

852

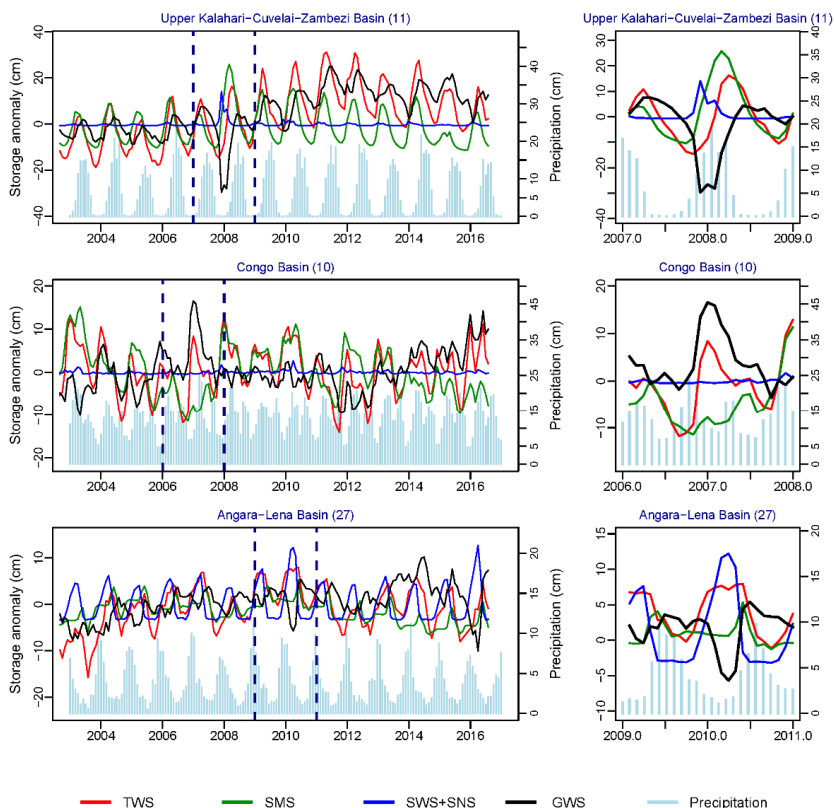


Fig. 6. Time series of ensemble mean GRACE Δ TWS (red), GLDAS Δ SMS (green), Δ SWS+ Δ SNS (blue) and computed GRACE Δ GWS (black) showing the calculation of anomalously negative or positive values of GRACE Δ GWS that deviate substantially from underlying trends. Three examples include: (a) the Upper Kalahari-Cuvélai-Zambezi Basin (11) under a semi-arid climate; (b) the Congo Basin (10) under a tropical humid climate; and (c) the Angara-Lena Basin (27) under a temperate humid climate; examples from an additional five aquifer systems under semi-arid and arid climates are given in the supplementary material (Fig. S75).



853

854

855

856

857

858

859

860

861

862

863

864

865

866

867

868

869

870

871

872

873

874

875

876

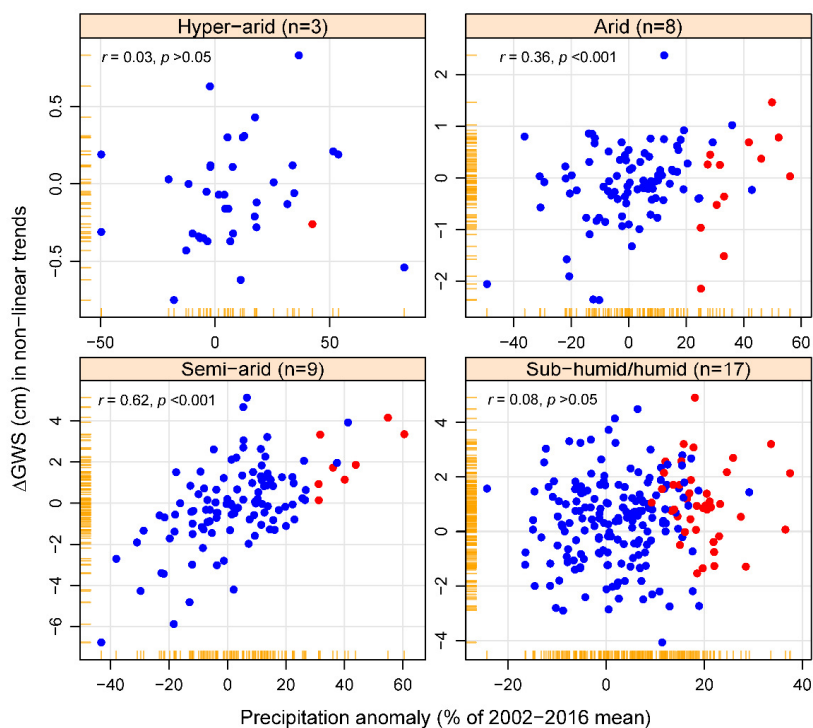
877

878

879

880

881



882 **Fig. 7.** Relationships between precipitation anomaly and annual changes in non-linear trends

883 of GRACE Δ GWS in the 37 large aquifer systems grouped by aridity indices; annual

884 precipitation is calculated based on hydrological year (August to July) for 12 of these aquifer

885 systems and the rest 25 following the calendar year (January to December); the highlighted

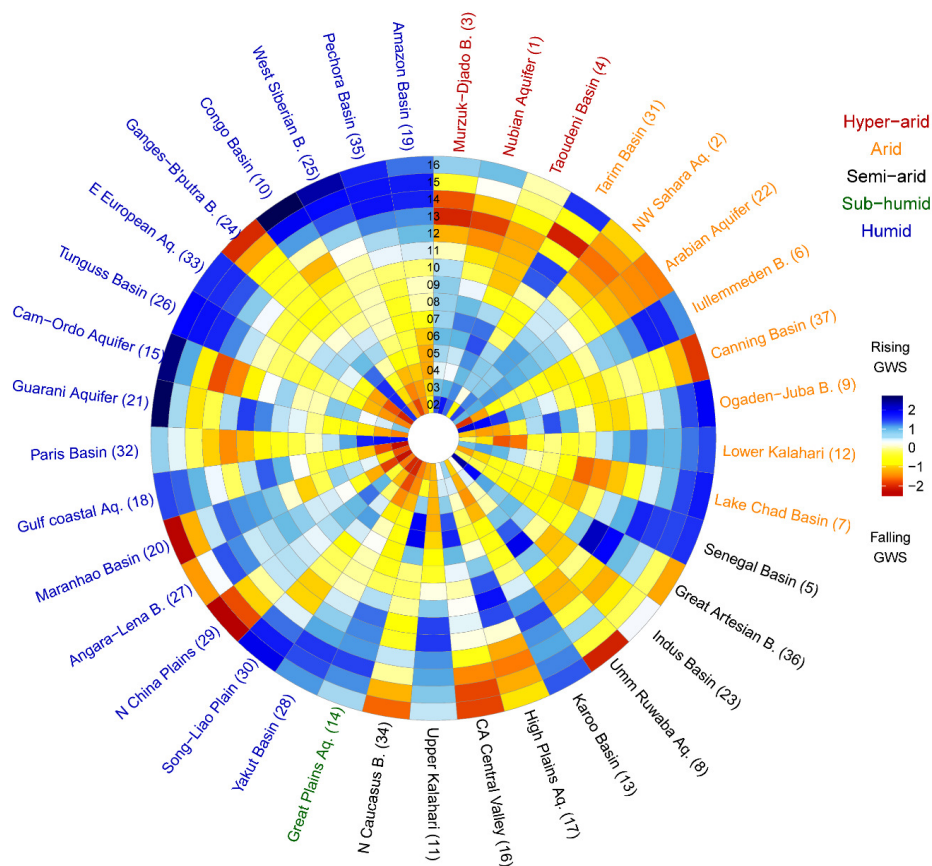
886 (red) circles on the scatterplots are the years of statistically extreme (>90th percentile; period:

887 1901 to 2016) precipitation.

888



889
 890
 891
 892
 893
 894
 895
 896
 897
 898
 899
 900
 901
 902
 903
 904
 905
 906
 907
 908
 909
 910



911 **Fig. 8.** Standardised monthly anomaly of non-linear trends of ensemble mean GRACE
 912 Δ GWS for the 37 large aquifer systems from 2002 to 2016. Colours yellow to red indicate
 913 progressively declining, short-term trends whereas colours cyan to navy blue indicate rising
 914 trends; aquifers are arranged clockwise according to the mean aridity index starting from the
 915 hyper-arid climate on top of the circular diagram to progressively humid. Legend colours
 916 indicate the climate of each aquifer based on the mean aridity index; time in year (2002 to
 917 2016) is shown from the centre of the circle outwards to the periphery.